Chinese Chemical Letters 33 (2022) 2658–2662

Contents lists available at ScienceDirect

Chinese Chemical Letters

journal homepage: www.elsevier.com/locate/cclet

Sn and Y co-doped $BaCo_{0.6}Fe_{0.4}O_{3-\delta}$ cathodes with enhanced oxygen reduction activity and CO_2 tolerance for solid oxide fuel cells

Nan Han, Rongzheng Ren, Minjian Ma, Chunming Xu, Jinshuo Qiao, Wang Sun, Kening Sun, Zhenhua Wang*

Beijing Key Laboratory for Chemical Power Source and Green Catalysis, School of Chemistry and Chemical Engineering, Beijing Institute of Technology, Beijing 100081, China

ARTICLE INFO

Article history:
Received 9 September 2021
Revised 25 September 2021
Accepted 28 September 2021
Available online 2 October 2021

Keywords:
Solid oxide fuel cells
Cathode
Heterovalent co-doping
Oxygen ion conduction
Oxygen vacancy formation

ABSTRACT

Applying mixed oxygen ionic and electronic conducting (MIEC) oxides as the cathode offers a promising solution to enhance the performance of solid oxide fuel cells (SOFCs). However, the phase instability in CO_2-containing air and sluggish oxygen reduction activity of MIEC cathodes remain a long-term challenge for optimizing the electrochemical performance of SOFCs. Herein, a heterovalent co-doping strategy is proposed to enhance the oxygen reduction activity and CO_2 tolerance of SOFCs cathodes, which can be demonstrated by developing a novel $BaCo_{0.6}Fe_{0.4}O_{3-\delta}$ (BCF)-based MIEC oxide, $BaCo_{0.6}Fe_{0.2}Sn_{0.1}Y_{0.1}O_{3-\delta}$ (BCFSY). In addition to improving the stability of BCF-based perovskites, this strategy achieves an optimized balance of ionic mobility and oxygen vacancies due to the synergies between the effects of the co-dopants. Compared with single-doped materials, BCFSY exhibits improved CO_2 tolerance and considerably higher ORR activity, which is reflected in a significantly lower polarization resistance of 0.15 Ω cm^2 at 600 °C. The results of this work provide an efficient tactic for designing electrode materials for SOFCs.

Solid oxide fuel cells (SOFCs), which can convert the chemical energy of fuels into electrical energy directly, have been deemed as promising power technology owing to their high chemical-to-electrical conversion efficiency, low environmental pollution, and the variety of potential fuels [1,2]. However, the high operating temperature of SOFCs hinders their practical application which not only rapidly degrades the electrochemical performance but also challenges the compatibility between cell components. The key to reducing the operating temperature is to develop robust and stable cathodes because the sluggish oxygen reduction reaction (ORR) at low temperature (LT) (500–650 °C) and the poisoning by pollutants widely occurred in ambient air such as CO_2 are the major challenges for achieving high electrochemical performance of SOFCs [3,4]. Therefore, there is a pressing need to develop suitable cathode materials with high ORR activity and extraordinary CO_2 tolerance.

The mixed ionic and electronic conductors (MIECs) that can broaden the fuel reactivity region from the three-phase boundary (TPB) to the entire cathode surface have gained extensive attention as cathode materials in which $BaCo_{1-x}Fe_xO_{3-\delta}$ (BCF) perovskite oxides are the most popular materials. These MIECs have attracted extensive research attention as cathode materials and are often used as attractive parent constituents for numerous cobalt-containing perovskite oxides [5,6]. Because of the large size and low divalent state of Ba^{2+}, these materials can offer adequate oxygen vacancies and lattice free volume to promote the migration of oxygen ions in the lattices of the perovskites [7]. Moreover, because of the inclusion of the transition metals cobalt and iron, which possess alterable valence states, BCFs demonstrate excellent catalytic activity. However, the phase structure of BCF is unstable. Owing to the large mismatch in ionic size between Ba and Co/Fe, these BCF-based perovskites change from a cubic phase to a hexagonal phase at low temperature. The resulting poor stability hinders the development of BCF-based cathode materials [8]. Consequently, stabilizing the phase structure of BCF-based materials is essential to fulfill the requirements of efficient cathodes for LT-SOFCs.

A mono-doping approach is often adopted to stabilize the cubic phase structure of BCFs. Cations with high or low valence have been doped into the partial B site to maintain the cubic phase structure of BCFs, such as Ta^{5+}, Y^{3+}, Sn^{4+}, Nb^{5+} [9–12]. Doping with cations at the B site increases the electrostatic repulsion between BO_6 octahedrons, and thereby promoting the formation of the cubic structure [13]. Unfortunately, although this mono-doping strategy demonstrates an effective approach to stabilize the structure of BCFs, it also leads to a high formation energy of oxygen

* Corresponding author.
E-mail address: wangzh@bit.edu.cn (Z. Wang).

https://doi.org/10.1016/j.cclet.2021.09.100
1001-8417/

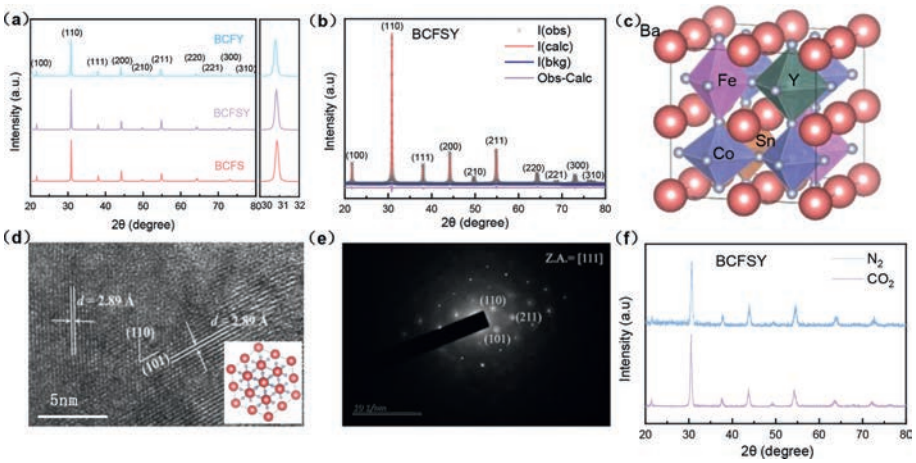

Fig. 1. Powder X-ray diffraction patterns and crystal structure. (a) XRD patterns of BCFS, BCFY and BCFSY samples. (b) Rietveld refinement of BCFSY XRD data. (c) Crystal structure of optimized BCFSY. (d) HRTEM image of BCFSY. (e) Corresponding SAED pattern. (f) XRD patterns of BCFSY after sintering at 700 °C in 20% CO_2 and N_2 for 24 h.

vacancies and sluggish oxygen ion migration. The stable valence ions occupying the Co position will destroy the continuity of the Co–O–Co (Fe) bond, and inevitably reduce its oxygen electron–ion conductivity, which decrease the catalytic activity of the cathodes to ORR [9]. The increase in the number of single dopants can improve the CO_2 tolerance at the expense of losing ORR activity.

Herein, we propose a new doping philosophy to enhance the ORR catalytic activity and the phase stability of BCF-based perovskite in CO_2-containing air, which is demonstrated by doping heterovalent metal ions (Sn^{4+} and Y^{3+}) into the B site of $BaCoFeO_3$ materials [$BaCo_{0.6}Fe_{0.2}Sn_{0.1}Y_{0.1}O_{3-\delta}$ (BCFSY)]. The doping of Y can change the electronic affinity and promote the generation of intrinsic oxygen vacancies. Moreover, doping Sn at the B sites of BCFs effectively activates the M–O bonds and improves the migration of oxygen ions. The synergetic effect of heterovalent co-doping can generate an optimized equilibrium of ion mobility and the generation of oxygen vacancies and thus yield excellent ORR catalytic activity. Compared to doping with a single metal element, the strategy of heterovalent co-doping can not only achieve excellent durability in air containing CO_2, but also provide superior oxygen ion conductivity, and thus embodies an advanced concept in the development of highly efficient cathodes for SOFCs.

To prove the successful incorporation of Sn and Y, X-ray diffraction (XRD) in air was first used to analyze the phase structure of the powders. All materials possess the perovskite crystal structure without any obvious impurity phases (Fig. 1a). The (110) diffraction peak in BCFY, BCFSY, and BCFS is found to gradually shift toward higher angles, indicating a decrease in the lattice volume, which can be ascribed to the slight difference in ionic radii of Sn and Y (Sn^{4+} = 0.069 nm, Y^{3+} = 0.090 nm). To obtain more information on the crystal structures of these materials, the acquired XRD information of BCFY, BCFSY, and BCFS in air were analysed via the Rietveld method (Fig. 1b, Figs. S1 and S2 in Supporting information). The low converged reliability factors (*e.g.*, R_p = 4.07%, χ^2 = 0.4206) illustrate that BCFSY can be divided into cubic perovskite structures (Fig. 1c) based on the space group Pm-3 m [14], and the lattice constant $a = b = c$ = 4.097 Å (Table S1 in Supporting information). The lattice volume increases in the trend BCFS < BCFSY < BCFY. Moreover, High-resolution transmission electron microscope (HRTEM) and their corresponding SAED patterns were used to further observe structural features (Figs. 1d and e). The crystalline fringes possess a lattice spacing of 2.89 Å, corresponding to the (110) and (101) crystal plane of the cubic phase structure. As seen in Fig. 1e, the SAED patterns near the center spot can be indexed to the (101), (211) and (110) planes in the view of the cubic unit cell, which further offer the evidence of the cubic structure of BCFSY. The results of the TEM and SAED show that the co-doping of Sn and Y can indeed stabilize the cubic phase structure of BCF.

The stability of the crystal structure, especially under low oxygen partial pressure and CO_2 atmosphere, is one of the important criteria for selecting suitable cathode materials [15,16]. To check the stability of BCFSY, the XRD pattern of three samples obtained at 700 °C under N_2/CO_2 for 24 h was compared. BCFSY still maintains its cubic perovskite structure when exposing in N_2/CO_2 atmosphere, without other obvious impure phases (Fig. 1f, Figs. S6 and S7 in Supporting information), confirming the phase stability of the BCFSY perovskite cathode.

The thermal expansion behavior is a crucial requirement for a stable performance of SOFCs. There should be a good match of the electrodes and the electrolyte in thermal expansion coefficient (TEC), otherwise the large difference in TECs between the SOFCs components may lead to internal stresses, which cause in performance degradation of the cathode. The TECs of BCFS, BCFY, BCFSY and SDC were measured (Fig. S9 in Supporting information). It can be seen that the TEC of BCFSY is 14.78 × 10^{-6} K^{-1} in the range of temperatures 150–1000 °C, which is lower than BCFS and BCFY. Besides, TEC of BCFSY is close to that of SDC (~12.6 × 10^{-6} K^{-1}) electrolyte, which is beneficial to the thermal stability of cathodes.

To investigate the electrochemical performance of BCFSY as an oxygen reduction electrode, symmetric cell configurations, *i.e.*, BCFSY|SDC|BCFSY, were constructed and tested in the temperature range of 500–650 °C (Fig. 2a and Table S2 in Supporting information). It displays the typical electrochemical impedance spectroscopy (EIS) plots of BCFS, BCFY and BCFSY electrodes. The polarization resistances of BCFS, BCFY, and BCFSY at 600 °C is 0.21, 0.29 and 0.15 Ω cm^2, respectively. It is clear that the polarization impedance (Rp) value of BCFSY is drastically decreased compared with those of BCFS and BCFY, revealing the outstanding ORR activity at low temperature. Moreover, the Arrhenius diagrams of the total polarization resistances of diverse samples (Fig. 2b) shows that the activation energies (E_a) of BCFY, BCFS, and BCFSY are 1.17, 1.15 and 1.10 eV, respectively. This strongly suggests that heterovalent co-doping can indeed significantly reduce the cathode polarization resistance, which is beneficial to the cathode ORR activity.

In addition, a Ni-SDC-based anode-supported single cell employing an SDC electrolyte has been fabricated to estimate the output performance of the BCFSY cathode [17]. The SDC electrolyte with a thickness of ~5 μm has a compact structure without connecting holes, ensuring a sealed operating environment (Fig. 2c).

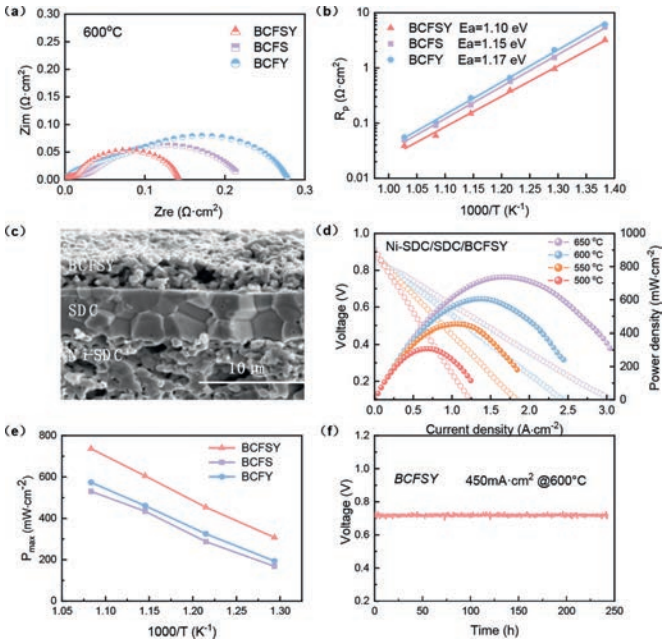

Fig. 2. (a) Impedance spectra of three samples at 600 °C. (b) The Arrhenius plot of the total polarization resistance of different cathode materials. (c) A typical SEM image of an anode-supported single cell with a Ni-SDC anode, SDC electrolyte and BCFSY cathode. (d) Typical *I*–*V*–*P* curves of BCFSY-based single cells. (e) Comparison of the electrochemical performance of single cells based on BCFS, BCFY and BCFSY at different temperatures. (f) Full cell durability test for the BCFSY-based single cell operated at 600 °C.

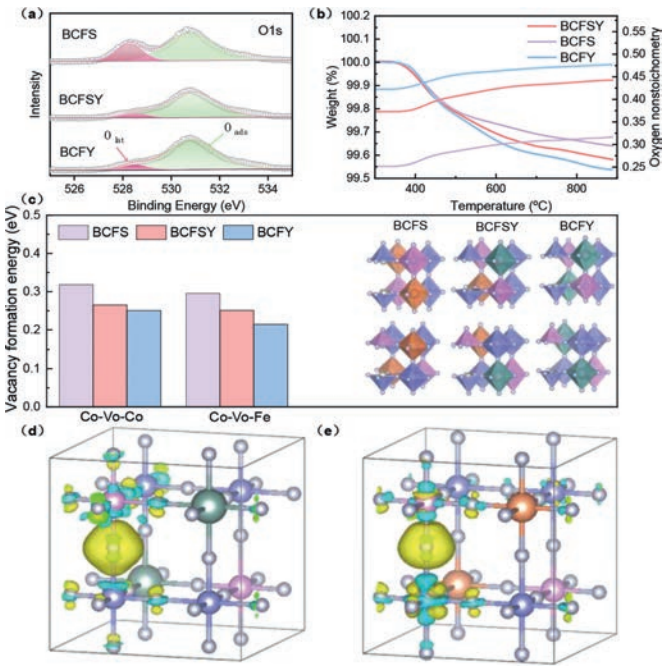

Fig. 3. (a) O 1s XPS spectra of the samples. (b) TG patterns and oxygen non-stoichiometry in the temperature range of 300–900 °C in air. (c) Oxygen vacancy formation energy for different types by DFT computations. (d) The charge density distribution map in BCFY. (e) The charge density distribution map in BCFS.

The cell with the BCFSY cathode attains a maximum power density of 736 mW/cm^2 at 650 °C (Fig. 2d), which is significantly greater than the power density obtained using the mono-doped cathodes (Fig. 2e). In addition, the power density is also significantly better than the BCFT (120 mW/cm^2) and BCFN (350 mW/cm^2) reported in the literature (Table S3 in Supporting information). The single cell also shows low EIS values (Fig. S10 in Supporting information), thus increasing the power density and resulting in the excellent performance of the BCFSY. Notably, the single cell retains an extremely durable voltage output for 240 h under a steady polarization current density of 450 mA/cm^2 at 600 °C (Fig. 2f), confirming that the BCFSY cathode can maintain outstanding ORR stability.

The performance of SOFC cathode mainly depends on the migration activity of O^{2-} [18]. In order to obtain a deep understanding of the superior ORR activity of BCFSY, the formation of oxygen vacancy and the activity of oxygen ion migration in the lattice of the materials were further studied. To analyze the formation mechanism of oxygen vacancy in BCFSY at room temperature, X-ray photoelectron spectroscopy (XPS) was initially carried out to acquire the information of O 1s in the three samples [19]. As shown in Fig. 3a, the peak at 528.3 eV is associated with the lattice oxygen (O_{lat}), while the peak at 530.7 eV can be assigned to the adsorbed oxygen species (O_{ads}) (Table S4 in Supporting information). The peak area of O_{ads} in the BCFY sample increases relative to BCFS and BCFSY. The increased proportion of O_{ads} indicates that the concentration of the adsorbed oxygen in BCFY increases, implying more oxygen vacancies are formed in BCFY [20,21]. The reduction of lattice oxygen in ABO_3 materials at high temperatures is another way for the formation of oxygen vacancies. The formation of oxygen vacancy can be represented according to Eq. 1:

$$2M_M^{\cdot} + O_O^{\times} \rightarrow 2M_M^{\times} + V_O^{\cdot\cdot} + 1/2O_2(g) \quad (1)$$

where $O_O^{\times}$ is the lattice oxygen and $V_O^{\cdot\cdot}$ is the oxygen vacancy. Therefore, thermogravimetric analysis (TGA) was conducted to further evaluate the concentration of oxygen vacancy and the loss of lattice oxygen based on the weight loss (Fig. 3b). BCFY results in more weight loss which indicate high oxygen non-stoichiometry, implying the high concentration of oxygen vacancy. To quantitatively analyze the oxygen vacancy concentration of the samples, the iodometric titration method was further measured (Table S5 in Supporting information). The oxygen non-stoichiometry (δ) in the materials increases in the trend BCFS < BCFSY < BCFY. This trend is consistent with the results of the XPS and TG analysis. Besides, it indicates that the doping of Y stimulates the formation of oxygen vacancies in BCFSY. Due to the charge compensation mechanism, the replacement of Y (3+) for Co/Fe can lead to the increase of the oxygen vacancy concentration in BCFY (Eq. 2).

$$2Y_2O_3 + 3M_M^{\times} + O_o^{\times} \rightarrow 4Y_M^{\prime} + V_o^{\cdot\cdot} + 3MO_2\ (M = Fe, Co, Sn) \quad (2)$$

To understand the Y^{3+}-doping on the formation of oxygen vacancies from an atomic point of view, first principles computations were implemented in $BaCo_{0.6}Fe_{0.2}Sn_{0.1}Y_{0.1}O_{3-\delta}$, $BaCo_{0.6}Fe_{0.2}Sn_{0.2}O_{3-\delta}$ and $BaCo_{0.6}Fe_{0.2}Y_{0.2}O_{3-\delta}$. The results of E_{form} are depicted in Fig. 3c and Table S6 (Supporting information). It is obvious that the formation energy of oxygen vacancy is the lowest in BCFY regardless of at Co-O-Co or Co-O-Fe, implying that the formation of $V_O^{\cdot\cdot}$ is easiest in BCFY. We can explicate the cause of this trend by analyzing the changes in the electronic structure during the formation of $V_O^{\cdot\cdot}$ [22]. As one oxygen vacancy is formed, two electrons are left behind in the perovskite and the two electrons related to oxygen ions are rearranged. Accordingly, the formation of oxygen vacancies depends on the electron affinity of the metal ions involved. To visualize the electron rearrangement in BCFS and BCFY, the charge density difference based on the ground state of DFT was computed (Figs. 3d and e). It is clear that the electronic density of the adjacent Co and Fe is changed by the leftover electrons from the oxygen vacancy. Hence, compared with BCFS, accepting electrons from the adjacent Co and Fe is easier owing to the presence of Y, which can explain why the oxygen vacancy formation energy of BCFY is the smallest. Combining the experimental results and theoretical calculations, we find that Y^{3+} excites the

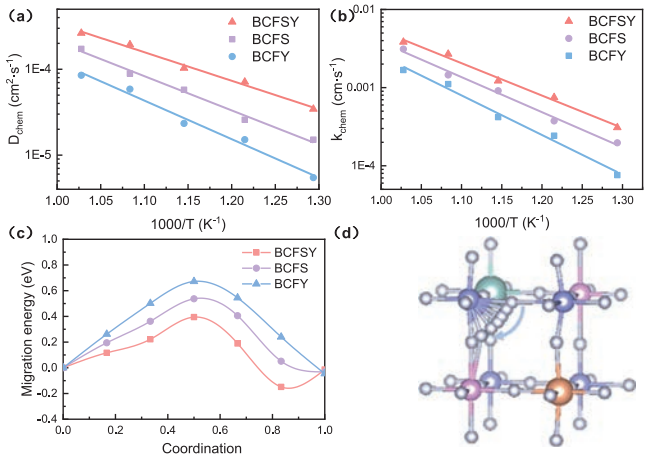

Fig. 4. (a) Temperature dependence of fitted D_{chem} from 500 °C to 700 °C. (b) Temperature dependence of fitted k_{chem} from 500 °C to 700 °C. (c) Calculated oxygen ion migration energy by DFT: migration barrier. (d) The migration path of the oxygen ion in BCFSY.

formation of oxygen vacancies by adjusting valence and electron affinity.

Identifying the oxygen-ion bulk diffusion coefficient (D_{chem}) and oxygen surface exchange coefficient (k_{chem}), which are determined through the electrical conductivity relaxation (ECR) method, is essential for evaluating the MIEC behavior of layered perovskites and can be helpful in assessing both the migration rate of oxygen ions and the electrochemical activity of cathode materials [23]. To illustrate the impact of Sn and Y heterovalent co-doping on MIEC performance, D_{chem} and k_{chem} are assessed through the ECR method (Fig. S13 in Supporting information) and the data are shown in Figs. 4a and b. In comparison, at 600 °C, the D_{chem} (1.03×10^{-4} cm^2/s) and k_{chem} (1.22×10^{-3} cm/s) values of BCFSY are much higher than BCFS and BCFY, and are superior to the BCFS reported in the literature (D_{chem}: 3.65×10^{-5} cm^2/s, k_{chem}: 2.23×10^{-4} cm/s). Although the oxygen vacancy formation energy and oxygen vacancy concentration of the co-doped material BCFSY are not the lowest, we find that this sample shows the highest D_{chem} and k_{chem}, which indicates that the oxygen vacancy concentration is not the only factor that determines the mobility of oxygen ions.

Apart from electron affinity, M–O bond strength is another contributor to the migration energy of O^{2-}. In order to explain how these factors synergistically effect the O^{2-} migration in Sn and Y co-doped system, the oxygen ion migration barriers were calculated (Figs. 4c and d, Table S7 in Supporting information) [24]. It can be found that the energy barrier of BCFS is lower than that of BCFY, even though the formation energy of oxygen vacancy is higher than that of BCFY. These results suggest that the lower bond strength of Sn-O than that of Y-O bond is the main reason for the low energy barrier of BCFS. The lower bond strength of Sn-O can be explained by the higher d occupancy rate of Sn^{4+} than Y^{3+}, which is good to the formation of a weaker polar covalent, donor–acceptor Sn-O bond with lower bond strength. Due to the coexistence of Sn^{4+} and Y^{3+} in BCFSY sample, it can synergistically tune both the electron affinity and M–O bond strength, thus endowing BCFSY with the lowest oxygen ion migration barrier (Table S7) and most remarkable electrochemical performance (Fig. 2b) among these three samples.

The high resistance to CO_2 poisoning of the SOFC cathodes matters a lot to the stable electrochemical output [25,26]. To demonstrate the durability of the BCFSY cathode in the presence of CO_2, the long-term stability of symmetrical cell configurations was tested in CO_2-containing air at an operating temperature of 600 °C.

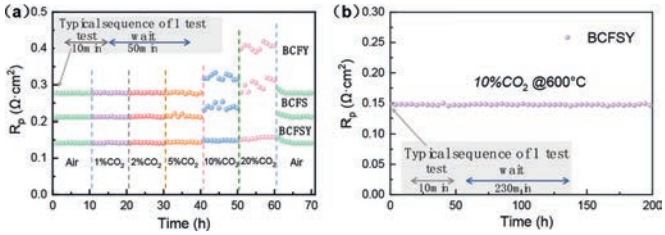

Fig. 5. (a) Time-dependent R_p values of BCFSY, BCFY, and BCFS cathodes treated in different CO_2 concentrations in air at 600 °C. (b) Durability test of a symmetric cell with the BCFSY cathode at CO_2 concentrations in air at 600 °C for 200 h.

As can be observed in Fig. 5a, the R_p values of BCFSY, BCFS, and BCFY electrodes remain steady at a CO_2 concentration of 1%–5%. Nonetheless, when the CO_2 concentration is increased to 10%, the R_p of BCFS increases from 0.211 Ω cm^2 to 0.253 Ω cm^2, and the R_p of BCFY increases from 0.274 Ω cm^2 to 0.329 Ω cm^2, whereas the R_p of BCFSY only changes from 0.144 Ω cm^2 to 0.147 Ω cm^2, which demonstrates the excellent stability of the BCSFY electrode. Moreover, when the CO_2 concentration is changed to 0, the R_p of all the electrodes returns to their original values after a period of time, implying that CO_2 does not render an irreversible impact on the electrode structure under the working conditions of the fuel cell. Besides, the short-term stability test of the BCFSY electrode under CO_2-containing air was further evaluated. As exhibited in Fig. 5b, a symmetric cell with the configuration of BCFSY|SDC|BCFSY demonstrates a stable R_p of around 0.147 after a 200 h operating period, clearly indicating that the BCFSY cathode has superior ORR activity and admirable CO_2 tolerance in 10% CO_2-containing air at 600 °C.

In conclusion, heterovalent co-doping perovskite BCFSY with stable phase structure was synthesized at low temperature. Comparing to BCFS and BCFY, BCFSY provides a favorable balance of oxygen vacancy content and ion mobility, which significantly improves the ORR activity. Accordingly, the highest power density, the distinguished durability in CO_2-containing air, and the lowest Ea values were observed with the BCFSY cathode. Consequently, the cathode with high ORR activity and excellent durability in air with CO_2 of BCFSY holds great potential for application in SOFCs. This doping philosophy also provides new possibilities for the application of clean and efficient energy conversion technologies.

Declaration of competing interest

The authors report no declarations of interest.

Acknowledgments

This work was financially supported by the National Natural Science Foundation of China (No. 22078022) and China Postdoctoral Science Foundation (No.2021M690379). We also thank Analysis & Testing Center, Beijing Institute of Technology for providing XRD equipment.

Supplementary materials

Supplementary material associated with this article can be found, in the online version, at doi:10.1016/j.cclet.2021.09.100.

References

[1] R. Ren, Z. Wang, C. Xu, et al., J. Mater. Chem. A 7 (2019) 18365–18372.
[2] D.D. Gu, Z. Guan, J. Guan, Chin. Chem. Lett. 32 (2021) 3548–3552.
[3] W. Jia, Z. Huang, W. Sun, et al., J. Power Sources 490 (2021) 229564.
[4] Y.H. Niu, W.R. Huo, Y.D. Yu, et al., Chin. Chem. Lett. 33 (2022) 674–682.
[5] R.Z. Ren, Z.H. Wang, X.G. Meng, et al., ACS Appl. Mater. Interfaces 12 (2020) 23959–23967.
[6] Y.J. He, X.F. Chang, X.L. Dong, et al., Chin. Chem. Lett. 19 (2008) 725–729.

[7] H. Zhao, N. Xu, Y. Cheng, et al., J. Phys. Chem. C 114 (2010) 17975–17981.
[8] C. Yang, Y. Gan, M. Lee, C. Ren, X. Xue, J. Electrochem. Soc. 165 (2018) F1032–F1042.
[9] S. Huang, Q. Lu, S. Feng, G. Li, C. Wang, Adv. Energy Mater. 1 (2011) 1094–1096.
[10] X. Yang, X. Han, T. He, Y. Du, Solid Oxide Fuel Cells (2017) 543–550.
[11] W. He, X. Wu, G. Yang, et al., ACS Energy Lett. 2 (2017) 301–305.
[12] P. Shen, X. Liu, H. Wang, W. Ding, J. Phys. Chem. C 114 (2010) 22338–22345.
[13] Y.F. Cheng, H.L. Zhao, D.Q. Teng, et al., J. Membr. Sci. 322 (2008) 484–490.
[14] X. Xu, C. Su, W. Zhou, et al., Adv. Sci. 3 (2016) 1500187.
[15] L. Zhang, J. Shan, Q. Wang, J. Alloy. Compd. 771 (2019) 221–227.
[16] W. Zhou, R. Ran, Z. Shao, W. Jin, N. Xu, J. Power Sources 182 (2008) 24–31.
[17] D. Lee, D. Kim, S.J. Son, et al., J. Power Sources 434 (2019) 226743.
[18] M. Li, M. Zhao, F. Li, et al., Nat. Commun. 8 (2017) 13990.
[19] M.J. Ma, J.S. Qiao, X.X. Yang, et al., ACS Appl. Mater. Interfaces 12 (2020) 12938–12948.
[20] C. Xu, K. Sun, X. Yang, et al., J. Power Sources 450 (2020) 227722.
[21] S.F. Xue, Y.J. Li, F.H. Zheng, et al., Rare Met. 40 (2021) 31–39.
[22] W.W. Zhang, L.F. Zhang, et al., J. Power Sources 446 (2020) 11.
[23] S. Choi, S. Sengodan, S. Park, et al., J. Mater. Chem. A 4 (2016) 1747–1753.
[24] Z. Du, H. Zhao, S. Li, et al., Adv. Energy Mater. 8 (2018) 1800062.
[25] Y. Chen, S. Yoo, Y. Choi, et al., Energy Environ. Sci. 11 (2018) 2458–2466.
[26] X.X. Yang, K.N. Sun, M.J. Ma, et al., Appl. Catal. B: Environ. 272 (2020) 8.